SCIENCE AND TECHNOLOGY OF ADVANCED MATERIALS, 2017
VOL. 18, NO. 1, 905–918
https://doi.org/10.1080/14686996.2017.1394776

Taylor & Francis
Taylor & Francis Group

FOCUS ISSUE REVIEW

OPEN ACCESS Check for updates

New chemistry of transition metal oxyhydrides

Yoji Kobayashi[a], Olivier Hernandez[b], Cédric Tassel[a] and Hiroshi Kageyama[a]

[a]Department of Energy & Hydrocarbon Chemistry, Graduate School of Engineering, Kyoto University, Kyoto, Japan;
[b]Solid State Chemistry and Materials Group, Institute of Chemical Sciences at Rennes, UMR 6226 CNRS-University of Rennes 1, Rennes, France

ABSTRACT

In this review we describe recent advances in transition metal oxyhydride chemistry obtained by topochemical routes, such as low temperature reduction with metal hydrides, or high-pressure solid-state reactions. Besides the crystal chemistry, magnetic and transport properties of the bulk powder and epitaxial thin film samples, the remarkable lability of the hydride anion is particularly highlighted as a new strategy to discover unprecedented mixed anion materials.

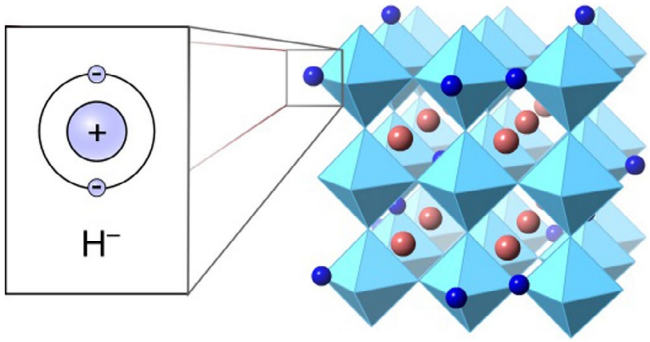

ARTICLE HISTORY
Received 16 May 2017
Revised 16 October 2017
Accepted 17 October 2017

KEYWORDS
Oxyhydride; hydride; mixed anions; solid-state chemistry

CLASSIFICATION
60 New topics / Others; 107 Glass and ceramic materials; 201 Electronics / Semiconductor / TCOs; 203 Magnetics / Spintronics / Superconductors

1. Introduction

In the early 1990s, the chemistry of metal oxyhydrides had been the subject of very scarce studies, mostly implicating electropositive *p*-group elements (eventually combined with transition metals to form an alloy) or more seldom intermetallic compounds containing non-metallic elements. Despite their very similar ionic radii (*ca.* 1.4 Å), the coexistence of hard oxide anions and soft, polarizable, hydride anions with a lower charge in a crystalline solid was usually considered as thermodynamically unlikely except under very reducing conditions able to stabilize the hydride anion [1].

The discovery of the very first mixed oxyhydride solid is considered as dating from 1982 with the solid-state synthesis at 900 °C under pure hydrogen of the ternary compound LaHO [2]. Subsequent X-ray and neutron powder diffraction experiments [3] pointed out that this material crystallizes in a fluorite superstructure featuring an ordered cubic anionic environment for lanthanum characterized by hitherto unseen oxygen–hydrogen contact distances of 2.85 Å. Such distances are specific of negatively charged hydrogen species, as they are much longer than the O^{2-}–H^{+} interatomic distance encountered in OH^{-} groups ranging from 1.32 to 1.37 Å. It is worth pointing out that LaHO turned out to be readily hydrolysable under ambient moisture, thereby releasing hydrogen. Later on, only few other stable materials containing both oxide and significant amount of hydride anions were reported, such as oxygen-stabilized η-carbides $Zr_3V_3OD_x$ (x_{max} = 4.93; D^{-} within Zr and V-tetrahedral interstices) [4] or $Zr_5Al_3O_{1-x}$, an oxygen-stabilized Nowotny phase able to uptake up to 4.8 interstitial hydride per formula unit [5]. One can also cite the inverse perovskite-type Ba_3AlO_4H [6] or the hydrogen-stabilized Zintl phase of barium $Ba_{21}T_2O_5H_x$ (T = Ge, Si, Ga, In, Tl; x_{max} = 24) [7] synthesized under drastically reducing conditions (1100 °C under a H_2 pressure of ~1 bar). In both latter compounds, isolated hydride occupies interstices inside distorted barium polyhedra.

CONTACT Yoji Kobayashi yojik@scl.kyoto-u.ac.jp; Olivier Hernandez olivier.hernandez@univ-rennes1.fr

Regarding more specifically transition metal oxyhydrides and anion substitution, thermodynamics suggest that only oxides with a strong formation enthalpy are prone to survive under reducing conditions and hence form oxyhydrides. Second, it should be recalled that the hydride itself is a very reducing chemical species, able to reduce the transition metal cation to the metal. Nonetheless, using a soft chemistry method ('chimie douce'), Rosseinsky et al. reported in 2002 the low temperature CaH_2 solid-state synthesis of $LaSrCoO_3H_{0.7}$ [8]. Contrary to the aforementioned examples of electropositive main group metal oxyhydrides, the chemical route at play here is of topochemical type—keeping intact the architecture of the layered perovskite reactants—and moreover in $LaSrCoO_3H_{0.7}$ cobalt–anion–cobalt pathways for magnetic exchange interactions are present. Interestingly, those pathways exhibit different strengths depending on whether an oxide or a hydride is locally present, allowing control of the electronic or magnetic properties. This new layered perovskite cobalt oxyhydride and its successors $LnSrCoO_{3+a}H_b$ with *Ln* = Pr, Nd [9] and $Sr_3Co_2O_{4.33}H_{0.84}$ [10] exhibit a rather low formal oxidation state for cobalt +1.7 and +1.75, respectively, that was considered as a stabilization condition for hydride-oxide systems [11]. The discovery in 2012 by Kobayashi et al. of an unanticipated $Ti^{3+/4+}$ barium oxyhydride, exhibiting hydride exchange and electronic conductivity [12], has renewed the chemistry of transition metal oxyhydrides. Here, the oxidation state of the *B*-site cation is not unusual, as many other Ti^{3+} compounds exist. Ever since, this family of materials has steadily grown, based on not only the topochemical route but also with the use of high-pressure solid-state reactions, extending the compositions to the Sc [13], V [14,15], Cr [16] or Mn [17] elements on top of the initial Co or Ti oxyhydrides.

The aim of this review is to present this new family of transition metal oxyhydrides, obtained by low temperature reduction with metal hydrides, or under high pressure and high temperature. Additionally, the synthesis, crystal chemistry, physical properties of the bulk powder and epitaxial thin film samples, and the remarkable lability of the hydride anion as a new strategy to discover unprecedented mixed anion materials will be presented.

2. Synthesis of oxyhydrides

The synthesis of oxyhydrides requires special care, given the unusual properties of the hydride anion. Preparation typically requires strongly reducing conditions, so excessive reduction of 3*d* cations to the metallic state may occur. Additionally, at high temperatures, many known hydride compounds decompose via H_2 release, so this is a potential issue in any oxyhydride compound. Treating oxides with H_2 typically only reduces the oxide to the metallic state at most; so far no syntheses of transition metal oxyhydrides from H_2 gas have been reported yet. Hence, the use of a hydride itself as a starting material is necessary; potential examples are the use metal hydrides such as CaH_2, NaH, and TiH_2, which may be commercially obtained or prepared in the lab by treating metals with H_2 gas at moderate temperatures. These starting materials are naturally useful in the synthesis of various Ca, Na, and Ti-containing transition metal oxyhydrides, but one is not bound to these compositions. For example, CaH_2 can be reacted with another oxide, and the resulting CaO can be removed from the reaction mixture by washing. These typically involve topochemical reactions. Hence, there are two main approaches to preparing oxyhydrides: the first involves the topochemical reduction of a parent oxide followed by removal of unwanted byproducts; the second involves a more direct synthesis from a mixture of hydride and oxide precursors, with no removal of intended byproducts. Recently, the latter has often been conducted under high pressure.

2.1. Topochemical synthesis

In solid-state chemistry, a topochemical synthesis is a synthesis based on the conversion of a parent compound converting to a product based on a very limited rearrangement of atoms, where the only bonds broken/formed are those which are necessary for the transformation. Topotactic reactions, a related but not necessarily exclusive term, signify that the overall symmetry of the structure before and after reaction are closely related. One simple example is ion exchange, whereby select atoms are exchanged while the other atoms do not diffuse and rather preserve the original crystal structure. Thus, unlike most high-temperature solid-state reactions, the structures of the starting materials and products of topochemical synthesis resemble each other quite closely. As low temperatures are involved and only 'minimal' changes to the structure are made, metastable products may also result. In terms of removing O^{2-} (for subsequent replacement with H^-) from oxides, the early work of Rosseinsky and Hayward [18–21], Kageyama [22–26], and Greenblatt [27] provides a starting point. For example, the three-dimensional (3D) perovskite $LaNiO_3$ can be treated with NaH at relatively low temperatures (200–300 °C) to yield the layered $LaNiO_2$ structure and $NaOH/Na_2O$, which is washed away [18]. The resulting $LaNiO_2$ structure resembles the original perovskite lattice, only in that selected 'apical' oxide anions have been removed. Similar novel oxygen-deficient structures have been reported for Mn [20,28], Fe [22–24] and Co [19,21]. Of course, these are not oxyhydrides, but the procedure for preparing oxyhydrides remains essentially the same.

The first transition metal oxyhydride, $LaSrCoO_3H_{0.7}$ (see Figure 1(a)) was prepared by the topochemical reduction of $LaSrCoO_4$ [8]. Other subsequent oxyhydrides which have been reported are titanates, such as (Ba, Sr, Ca, Eu)$TiO_{3-x}H_x$ [12,29,30] (structure shown in Figure 1(b)),

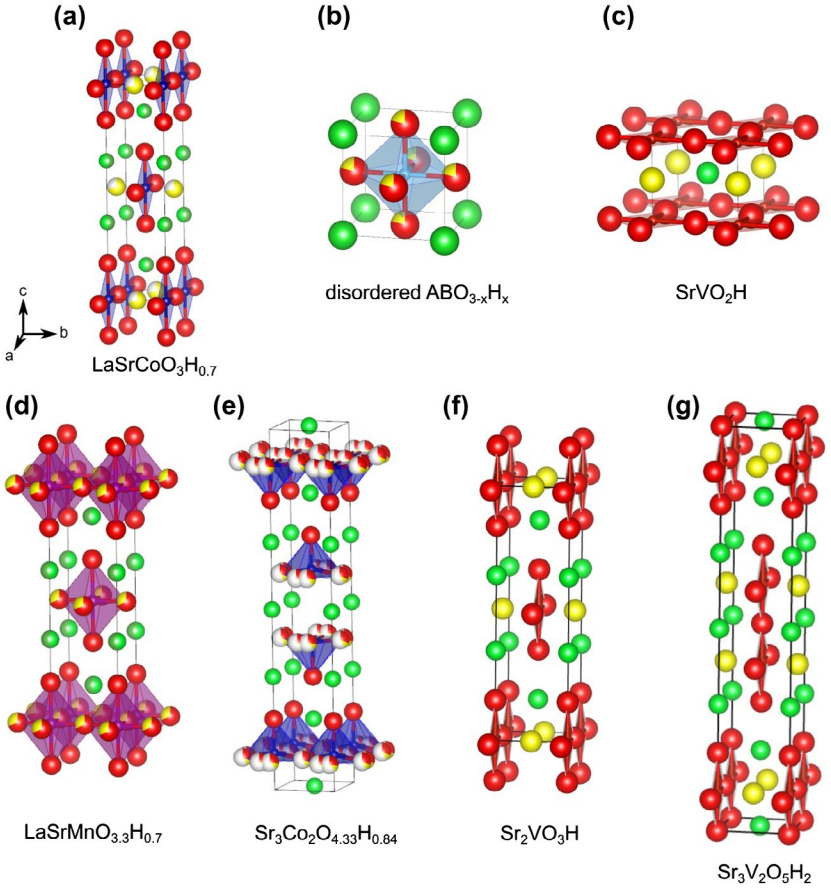

Figure 1. Structures of various oxyhydride compounds. For all structures, unit cells are oriented in the same *a*, *b*, *c* direction, as indicated in (a). Hydride is shown by yellow spheres, and oxide by red spheres. For the layered structures, interlayer La and Sr cations are shown by shades of green. For disordered $ABO_{3-x}H_x$ in (b), the primitive cubic cell seen with $BaScO_2H$, $SrCrO_2H$, $SrTiO_{3-x}H_x$, and $BaTiO_{3-x}H_x$ is shown; octahedral tilting is observed for certain Ca-Sr solid solutions $(Ca,Sr)TiO_{3-x}H_x$, resulting in larger unit cells (not shown).

and vanadates, such as $SrVO_2H$ [15] (Figure 1(c)). All of these examples involve grinding the parent oxide with CaH_2 and pelletizing within a glovebox, followed by sealing in an evacuated glass ampoule. Heating to 300–600 °C results in the oxyhydride product and CaO by-product, the latter of which is washed away in a methanol solution of weak acid (ammonium chloride). This method has also been applied to the preparation of oxyhydrides in thin form. Typically the parent oxide ($SrTiO_3$, $LaSrCoO_4$, etc.) is deposited on a suitable substrate via vacuum techniques such as pulsed-laser deposition. The film/substrate is then treated in the same way as powder, by immersion in loose CaH_2 powder and sealing in a Pyrex tube under vacuum. Consequent heat treatments can be conducted at slightly lower temperatures. In this way, films of (Ba, Ca,Sr) $TiO_{3-x}H_x$ [31,32] and $LaSrCoO_{4-x}H_x$ [33] have been prepared.

While not being a transition metal oxyhydride, we note that the interesting calcium aluminate oxyhydride C12A7:H^- is also formed from its parent oxide (C12A7 for mayenite $12CaO \cdot 7Al_2O_3$) either by reaction at 1300 °C with 20% H_2/80% N_2 [34] or alternatively using a CaH_2 reduction process at 800 °C leading typically to a higher hydride content than the high-temperature solid–gas route [35]. For the titanate cases, the amount of hydride can be varied within $x = 0$–0.6 for a $BaTiO_{3-x}H_x$ formula by adjusting the temperature and CaH_2 amount. However, increasingly strenuous conditions eventually lead to decomposition of the original oxide framework, observed in terms of reduced crystallinity and increasing amounts of TiH_2 [12]. We further note that it is not yet possible to predict whether an oxygen-deficient product or oxyhydride product will result; for example, an anatase TiO_2 film simply gives a dark-colored TiO_{2-x} phase when treated with CaH_2 [36], whereas $BaTiO_3$ gives the oxyhydride. $La_2Ti_2O_7$ contains only minute amounts of hydride [37].

Most hydride reductions to date have used CaH_2, with fewer examples with NaH and LiH. We can see that the surrounding thermodynamics differ when using these various hydrides [38]. For example, in the absence of any oxide to reduce, NaH and CaH_2 will decompose at high temperatures:

$$NaH\,(s) \rightarrow Na\,(l) + \tfrac{1}{2}\,H_2(g) \qquad (1)$$

$$CaH_2(s) \rightarrow Ca(s) + H_2(g) \qquad (2)$$

As Ca^{2+} is a divalent cation, the lattice enthalpy of CaH_2 is considerably higher than that of NaH. Thus, while at

210 °C a H_2 pressure of 10 Torr may result, the equilibrium constant for eq. 2 is predicted to be only 10^{-8} even at 400 °C (assuming $\Delta H°$ and $\Delta S°$ values are independent of temperature). Hence, CaH_2 is probably suitable at a higher temperature rather than NaH, otherwise, the experiment simply becomes a reduction using pure Na or Ca metal. Obviously, a suitable reduction temperature also depends on how easily the target oxide can be reduced (e.g. Fe vs. Ti), but the trend above still holds.

In comparing these hydride reducing agents, it is also necessary to compare the thermodynamics of the by-products. For example, a reduction with NaH could possibly yield either Na_2O or NaOH; similarly, CaH_2 could yield either $Ca(OH)_2$ or CaO. The question in essence here is whether a one-electron or two-electron reduction is involved [38], that is,

$$H^- \rightarrow H^+ + 2e^- \quad (3)$$

$$H^- \rightarrow {}^1/_2H_2 + e^- \quad (4)$$

In reality, NaOH is quite stable compared to Na_2O, as demonstrated for example by the extreme difficulty of dehydrating NaOH to Na_2O. Hence, reductions with NaH probably result in the two-electron reduction, yielding NaOH rather than Na_2O. Another further point to consider is the side reaction between any hydroxide by-product and remaining hydride:

$$NaH + NaOH \rightleftarrows Na_2O + H_2 \left(K_{eq,400°C} = 10^{-6} \right) \quad (5)$$

$$Ca(OH)_2 + CaH_2 \rightleftarrows 2CaO + 2H_2 \left(K_{eq,400°C} = 10^{12} \right) \quad (6)$$

For NaH, the small K_{eq} of Equation (5), combined with the dominance of Equation (3) over Equation (4) imply that any hydrogen pressure during the experiment is the result of a thermal decomposition (Equation (1)), rather than reduction of the parent oxide. This should be taken into account during synthesis, as the experiment may be more sensitive to reaction temperature and ampoule volume.

In the case of CaH_2, only a small amount of H_2 will be released from thermal decomposition. Rather, H_2 will be released from either one-electron reduction of the oxide (Equation (4)), or any $Ca(OH)_2$ impurities with the CaH_2. Depending on the reactant quantities, this pressure can be substantial (up to 20 atm), leading to minor explosions. The effect of H_2 pressure on the oxyhydride formation has been briefly discussed previously [9], and should be taken into account when standardizing experimental procedures. Gas-phase contributions toward the formation of oxygen-deficient oxides using CaH_2 and NaH have been demonstrated in the past [18,38].

The benefits of these topochemical hydride synthesis are the relative ease (compared with the next method) in terms of equipment. Additionally, synthetic explorations are simple to plan, where one may choose any (in theory) oxide where one believes that there is O^{2-} which may be removed/exchanged, and the products typically do not yield multiple phases or drastically different crystal structures, making structural analysis straightforward. The drawback, however, lies in the inherent *reduction* nature of the process itself; that is, for the reaction to occur, the transition metal must undergo a reduction. For example, $BaTiO_3$ (Ti^{4+}) is reduced to $BaTiO_{2.5}H_{0.5}$ ($Ti^{3.5+}$). Zr, however, is considerably more difficult to reduce, and the synthesis of $BaZrO_{2.5}H_{0.5}$, or other irreducible elements such as Sc or Al is difficult to conceive. Hence, while there are still no Nb, Ta, or W oxyhydrides reported so far, for example, the exploratory space is eventually limited by the repertoire of parent oxide. Additionally, over-reduction can also occur; our attempts to prepare iron-based oxyhydrides almost always result in the formation of Fe metal.

2.2. Direct synthesis via high pressure

A direct synthesis of transition metal oxyhydrides without any redox processes eliminates the problems encountered above for topochemical reductions. Hypothetically, $BaTiO_2H$ could be synthesized by reacting stoichiometric amounts of BaH_2, BaO, and Ti_2O_3. The method can be used to achieve compositions based on irreducible elements, such as $SrAlO_2H$. However, BaH_2 and other simple hydrides often decompose to release H_2 gas at the elevated temperatures necessary to achieve these solid-state reactions. The use of solid-state high-pressure techniques eliminates this problem by enclosing the reaction mixture in a solid container with virtually no head space; heating under these conditions prevents the loss of hydrogen, making oxyhydride synthesis possible. A sample cell is shown in Figure 2. To form a gas-tight seal, care must be taken in choosing the cell materials. In our own research, we have found that Au and Pt components seem to react with alkali/alkali earth reagents. NaCl sleeves work well, as they are soft enough to fuse into gas-tight seals under pressure, unlike other materials such as BN or Pt foil. NaCl has the additional advantage in that it may be removed by washing. Supplementary sources of H_2 can be included within the cell, as with a mixture of $NaBH_4/Ca(OH)_2$ [14]. The high-pressure technique has been quite successful in forming the oxyhydride compounds; to date Sr_2VO_3H [14], $SrCrO_2H$ [16], $LaSrMnO_{3.3}H_{0.7}$ [17], and $BaScO_2H$ [13] have been reported (see Figure 1).

3. Specificity of oxyhydride characterization

Generally speaking, hydride as a negatively charged hydrogen atom should be characterized as any hydrogen species in a solid. The difficulty to chemically and structurally characterize transition metal oxyhydrides depends obviously on the level of hydride content in

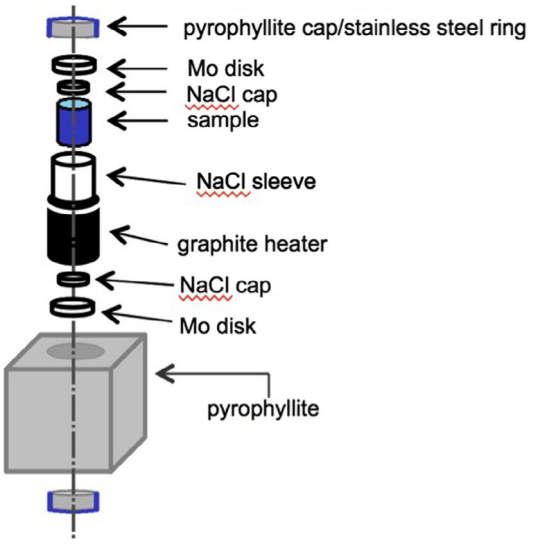

Figure 2. Schematic of a sample cell for high-pressure of oxyhydrides. The pyrophyllite cube is approximately 1.5 cm × 1.5 cm × 1.5 cm. Tungsten carbide blocks (anvils) apply pressure to the pyrophyllite cube from all six faces. Heating is achieved by electric current, via electrical contacts running through the tungsten carbide anvil, steel ring, and Mo disk to the graphite heater.

the investigated material. For oxyhydrides prepared by direct synthesis, an initial estimation of the hydride content can be made based on the reaction stoichiometry, but for topochemical reactions the amount of hydride will depend on the temperature and duration of the CaH_2 reduction step. Furthermore, at the crystal-averaged atomistic level, the location of hydride anions in the unit cell may be difficult to identify owing to the ordered or disordered character of the anionic sublattice. In the latter case, the presence of H^- on an anionic site also statistically occupied by an oxide anion is not so straightforward to ascertain and it is quite easy to miss. In fact these three species, hydride, oxide and vacancies, can in principle be present in the material and thus can coexist on the same crystallographic site, constituting a complex situation. Moreover, the simultaneous presence of hydroxide molecules coexisting with hydride anions is also possible in metal oxides or calcium phosphates as brought up recently by Hayashi et al. by nuclear magnetic resonance (NMR) [39] or based on maximum entropy method (MEM) analysis of neutron diffraction data by Masuda et al. [40]. The combined use of different characterization techniques is therefore highly required. The sought chemical composition is actually dependent on several assumptions, for instance, the correctness of the mass fractions refined by Rietveld analysis in case of coexisting phases and the oxygen stoichiometry of the eventually remaining starting pure oxide. These highlight the difficulty to get an unambiguous chemical and structural description of highly disordered oxyhydrides. We summarize below most of the techniques used so far for characterizing oxyhydrides, underlining their respective advantages and disadvantages.

Diffraction techniques, namely laboratory or synchrotron X-ray powder diffraction (XRD) as well as neutron powder diffraction (NPD), are widely used to investigate the structure and composition of obtained products. Clearly NPD, although not always accessible within a reasonable period of time, is required for a correct structural analysis of oxyhydrides as XRD is not able to detect hydrogen in the presence of heavy elements (e.g. Sr, Ba, La, Pr, Nd etc.). For Eu [30,41], or other highly absorbing elements (e.g. Sm, Gd, Dy) NPD should be nonetheless avoided, though not impossible with a special cell arrangement [41]. High-resolution time-of-flight (TOF) NPD instruments are often more suited than constant-wavelength diffractometers to determine subtle structural features, for instance coexistence of O^{2-} and H^- on the same site, as shown in $LnSrCo_{3+\alpha}H_\beta$ oxyhydrides (*Ln* = Pr, Nd) [9]. A combined Rietveld refinement of XRD and NPD data collected at the same temperature allows a structural model more robust and less prone to least-squares correlations between occupancy and atomic displacement parameters, as they help in benefitting from very different atomic scattering factors of each chemical species with X-rays and neutrons. Such an approach is particularly useful to demonstrate the hydride location and the chemical occupancies of each site [8,12]. The eventual presence of impurity phases plus small amount of starting material may make the multi-phase Rietveld refinement challenging. It is worth noticing it is not always possible to exclude by diffraction the possible presence of a low amount of oxide anions on a hydride site. If resulting metal-O bond length is rather short (e.g. 1.80 Å vs. 2.18 and 1.94 Å for the pure oxide O1-apical and O2-equatorial sites in $LaSrCoO_3H_{0.7}$ [8]) this assumption can be reasonably discarded, by relying also on chemical analysis results.

In the course of the structural determination of $LaSrCoO_3H_{0.7}$ [8], a pure oxide, without hydride anion, was first proposed from synchrotron XRD data according to an *Immm* Sr_2CuO_3-type model consisting of chains of corner-sharing CoO_4 squares. Intuitively, it would correspond to a reductive topotactic transformation from $LaSrCo^{+III}O_4$ (octahedral cobalt) into the $LaSrCo^{+I}O_3$ structure (square planar cobalt) during which the oxide anions which connect the octahedra in the *b* axis within the equatorial plane were removed in an ordered manner (see Figure 1(a)). While NPD gave a satisfactory fit for magnetic reflections, the nuclear peaks remained still poorly modeled by the *Immm* $LaSrCoO_3$ structural model. A difference Fourier map showed the presence of a substantial hole of negative nuclear density at these sites. As hydrogen is one of five natural elements to exhibit a negative coherent scattering length (together with Li, V, Ti and Mn), it was successfully incorporated in the model at this position, yielding in a greatly improved refinement.

In a similar manner, for $BaTiO_{3-x}H_y$ [12] it was the significant discrepancy between the oxygen content refined from the synchrotron XRD data and from the NPD data on the other hand that led to suspect the presence of hydride. Initially, after reduction of $BaTiO_3$, a refined stoichiometry of $BaTiO_{2.59(6)}$ was obtained from synchrotron XRD data. An independent refinement of the NPD data led to a much lower oxygen content ($BaTiO_{1.91(3)}$), corresponding to an unrealistic Ti valence of +1.82. Such discrepancy in terms of oxygen content derived from NPD and XRD diffraction experiments could be explained only by the presence of negative-scattering hydrogen randomly disordered with oxide on the single anionic site, decreasing the apparent nuclear density of this site with respect to the initially calculated density. If only oxygen is considered by NPD Rietveld (ignoring hydrogen) its content is then underestimated, while by XRD—insensitive to the presence of hydrogen—the oxygen content is correctly determined, although intrinsically less accurate as oxygen is a light element for X-rays in presence of heavy elements. Introducing hydrogen on the anionic site and refining again the NPD data alone increased the oxygen content to $BaTiO_{2.33(2)}$, a value much closer to the one obtained by synchrotron XRD. A combined Rietveld refinement of XRD and NPD data was conducted to obtain the final refined formula, $BaTiO_{2.38(1)}H_{0.62}$. NPD allowed additionally to discard the presence of hydroxide molecules in the solid as Fourier difference maps did not show any significant negative holes at around 1 Å from the anionic site. Based on the agreement of X-ray and neutron refinement data with a model consisting of only hydride and oxide at the anionic site, the combination of these two data-sets also revealed the total or almost total absence of vacancies.

The MEM applied to powder neutron diffraction data [42]) is in principle more accurate than conventional Fourier difference maps, leading to less biased nuclear density maps with less background. Figure 3(a) shows a neutron diffraction pattern of a $BaTi(O^{2-}, D^-, OD^-)$, and a nuclear density map based on MEM analysis in Figure 3(b). Small spots of nuclear density are observed approximately 1 Å from the oxygen centers signifying the presence of hydroxide (in deuterium form). In contrast, MEM analysis of $BaTiO_{2.4}D_{0.6}$ does not exhibit any such lobes (Figure 3(c)). Thus, this method was able to suggest the stable coexistence of H^+ and H^- at ambient conditions in $BaTiO_{2.4}(D^-)_{0.3}(OD^-)_{0.3}$ [40], and a subsequent combined Rietveld refinement of neutron and X-ray diffraction data was used to obtain the precise anionic stoichiometry.

Other techniques than diffraction are used to qualitatively and quantitatively determine the hydride content in oxyhydrides. For example, mass spectrometry (as typically encountered in a TG-MS setup) can be used. The presence of hydride in $LaSrCoO_3H_{0.7}$ [8] was chemically confirmed by quantitative mass spectrometric monitoring of the H_2O evolved simultaneously with oxidation of the oxyhydride material under flowing O_2(g) at 272 °C, yielding 0.4 H^- per formula unit, a value almost half of the hydride stoichiometry determined by diffraction. Of course, heating hydroxides also yields H_2O, so the release of H_2 when heating under inert atmospheres such as Ar or He can be taken as an indication of hydride within the lattice [12]. Quantification of hydride is not trivial, but may be accomplished with rigorous use of internal standards within the gas stream and standard hydride samples. Another approach to quantification has been acid digestion of the sample, and volumetric/mass spectrometric analysis of the evolved gases. For example Yoshizumi et al. and Kobayashi et al. dissolved their C12A7:H^- [43] and $BaTiO_{3-x}H_x$ samples [12] in DCl/D_2O or D_2SO_4, and collected the evolved gases to prove and quantify the existence of lattice hydride.

As a related technique to heating the sample under inert atmospheres and measuring the released H_2 gas, thermal desorption spectroscopy [44] has also been used as a characterization tool. This typically requires a dedicated instrument, composed of a high vacuum chamber, in-line mass spectrometer, and IR heating stage. Quantification is possible with careful calibration, and was used by Bouilly et al. [33] and Bang et al. [14] for their thin film and powder samples.

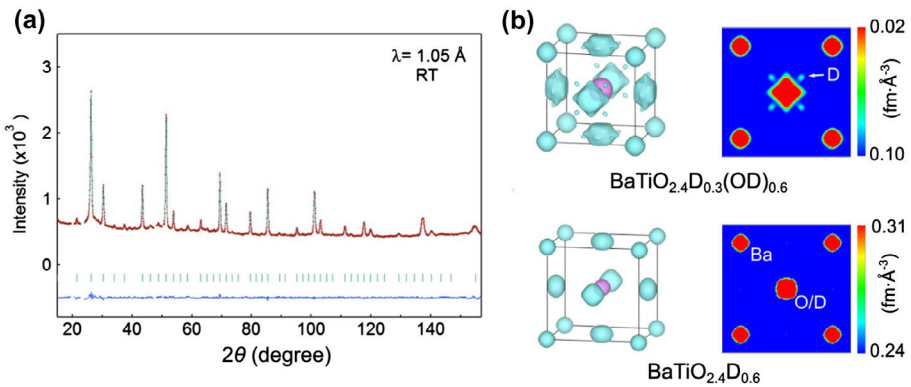

Figure 3. Neutron diffraction pattern (a) and nuclear density maps from MEM analysis (b) to differentiate anionic species.

Thermogravimetry analysis (TGA) can be used under oxidative atmosphere to confirm the suspected stoichiometry via weight change. Any oxyhydride obtained by topochemical reduction can be reoxidized to the original parent oxide, undergoing a weight change reflecting the original hydride content, assuming there are no anion vacancies. For $BaTiO_{3-x}H_y$ [12] the refined formula from Rietveld analysis, $BaTiO_{2.38(1)}H_{0.62}$, compares nicely well with the one deduced from TGA in air, $BaTiO_{2.38}H_{0.62}$. Reductive TGA may also be performed; for $Sr_3Co_2O_{7-y}H_y$ [10] the observed relative mass loss by reductive TGA under 5%H_2 in N_2 was used (in combination with other results) to confirm a $Sr_3Co_2O_{4.33}H_{0.84}$ formula.

TGA experiments revealed in $LnSrCo_{3+\alpha}H_\beta$ oxyhydrides (*Ln* = Pr, Nd) an oxygen stoichiometry substantially higher than 3.0 (up to 3.33) [9], contrary to $LaSrCoO_3H_{0.70}$. Based on this additional information, extra oxide anions were introduced in the crystallographic model on or very close to the hydride site bridging the cations in the *ab* plane. This implied that the substitution of oxide for hydride within the $CoOH_{1-x}$ sheet was incomplete in those Pr- and Nd-containing cobalt oxyhydrides; the additional substitutional disorder in the transition metal layer induced local variations in the Co environment such as displacements of the pure oxide O2 equatorial site handled by a 'split-atom' model.

Simple, routine elemental analysis using commercial CHN analyzers can play an important role to quantitatively confirm the results from NPD/synchrotron XRD combined Rietveld refinement. Regarding $LaSrCoO_3H_{0.7}$ [8] a more accurate global hydrogen content was obtained by elemental analysis, revealing 0.26(2)% H by mass, very close to the 0.21% mass from the combined Rietveld refinement, definitely confirming the absence of oxide anion on the hydride site, which is statistically occupied by only hydrides and vacancies. ^{1}H magic angle spinning nuclear magnetic resonance spectroscopy (MAS NMR) qualitatively confirmed the presence of hydride in the $Sr_3Co_2O_7$ majority phase by comparison with a CaH_2 spectrum [10]. ^{1}H MAS NMR measurements otherwise confirmed the same chemical state and environment for hydrogen species in $BaTiO_{3-x}H_y$ [12]. As mentioned above, H^-/OH^- are not so simple to differentiate by NMR (see the recent study by Hayashi et al. [39]). But this spectroscopic technique remains one of the few tools for exclusively seeing hydrogen and its position, though not so usable if one deals with magnetic or conducting samples.

Use of H/D isotopes can help when dealing with neutron diffraction or mass spectrometry. The H^- and D^- exchange within $BaTiO_{3-x}H_y$ was shown to occur in D_2(g) atmosphere at 400 °C monitored *in situ* by MS, confirmed by NPD experiments before and after deuteration [12].

The valence of the transition metal can be checked by Curie–Weiss fitting against magnetic susceptibility data, on the other hand X-ray absorption spectroscopy (XAS) is also used to confirm the formula. The average oxidation state of Co calculated from the refined anionic content in $LaSrCoO_3H_{0.7}$ [8] was shown to be consistent with an X-ray absorption Co *K*-edge position very close to that of the Co(II) standard ($LaSrCoO_{3.5}$). In $BaTiO_{3-x}H_y$ magnetic susceptibility data showed a +3.4 oxidation state for Ti strengthening more the refined formula [12].

Muon spin rotation (μSR) experiments confirmed $LaSrCoO_3H_{0.7}$ was magnetically ordered [8] and quasi-elastic neutron scattering experiments [45] were carried out to probe dynamics of the same material within the –0.4 and 0.4 meV energy transfer window with an instrumental resolution of 17.5 meV in FWHM. This corresponds to a timescale of 1–75 ps. The onset of hydride mobility along the *a* axis within the perovskite layer was revealed above 402 °C, associated with an ionic conductivity of *ca.* 3–5 S cm^{-1} around 427 °C, significantly higher than in protonic conductors.

Besides the different relevant techniques mentioned hereinabove (XRD, NPD, TGA, MS, magnetic susceptibility, NMR, XAS, chemical analyses etc.), hydrogen forward scattering (HFS) [46] can also be cited as another experimental method used so far for the analysis of TM oxyhydrides [30], quantification requiring curve fitting.

As far as they are concerned, epitaxial thin films of $ATiO_{3-x}H_x$ (*A* = Ba, Sr, Ca) [31] were characterized by XRD and by secondary ion mass spectroscopy (SIMS). Low temperature CaH_2 reduction and subsequent hydride insertion was shown to induce small change in unit cell parameters relative to the as-grown oxide film. SIMS, that is an expensive technique and requires standards for quantification but compulsory for thin films, gave hydrogen density (that turned out to be large, e.g. $SrTiO_{2.75}H_{0.25}$) and its depth dependence, pointing out a uniform distribution in the film.

4. Chemical reactivity of oxyhydrides: lability and exchange

The chemical reactivity of hydride is unlike that of any other anion. The redox potential of H^- between H_2 and H^- is highly negative (–2.23 V). Thus, H^- can be readily oxidized to H_2 gas. The oxidant may be an external species, or one of the metal cations within the compound itself; the latter is more conveniently described as a reductive elimination of hydride. This property is illustrated in the release of H_2 from TiH_2 when heated at approximately 400 °C, for example [47,48].

This release of H_2 can also be seen in certain oxyhydrides, and in reversible manner. Using a TG-MS apparatus under flowing Ar, Kobayashi et al. observed the release of H_2 from $BaTiO_{2.4}H_{0.6}$ at approximately 400 °C during a linear temperature ramp from room temperature to 600 °C (and presumably yielding a $BaTiO_{3-\delta}$ product, see Figure 4). Repeating the experiment under D_2 gas led to the detection of HD gas, also peaking at 400 °C. The oxyhydride product was found to be almost

fully deuterated (based on neutron diffraction), indicating that hydride exchange with gaseous hydrogen is possible at 400 °C, the same temperature as the release temperature.

This demonstrated thermolability of hydride is quite interesting as it makes anion exchange possible. In solution chemistry, the broad range of various inorganic complexes rests upon the fact that various (precursor) ligands are *labile*, that is, they do not bind too strongly neither too weakly, making consequent ligand exchange possible. Hydride in oxyhydrides appears to be of similar use. Other than the thermal lability described above, we note that H^-, as a base, would also be prone to acid-base reactions with acids, also permitting it to leave as H_2 gas under moderate conditions.

The thermal lability for synthetic purposes has been demonstrated by Yajima et al. [49] and Masuda et al. [40] recently by their synthesis of oxynitride $BaTiO_{3-x}N_y$. Typically, the preparation of oxynitrides has required the use of NH_3 at high temperatures of 800–1300 °C. In the case of preparing the oxynitride version of $BaTiO_3$, the highest nitrogen content has been $BaTiO_{2.85-\delta}N_{0.1}$ which was prepared with flowing NH_3 at 950 °C. In contrast, by the use of a $BaTiO_{2.4}H_{0.6}$ precursor, treatment with NH_3 at temperatures of 375–550 °C led to considerably higher nitrogen contents of $BaTiO_{2.4}H_{0.3}N_{0.1}$ – $BaTiO_{2.4}N_{0.4}$. Furthermore, Masuda et al. [40] have reported that even N_2 can yield oxynitride $BaTiO_{2.5}N_{0.2}$ at 500 °C. Presumably, once the labile hydride anion leaves, the Ti cation becomes coordinatively unsaturated, and thus becomes active enough to react with N_2 gas despite its triple N–N bond.

Apart from the thermal lability, an acid-base reaction involving hydride has also been invoked to yield new mixed-anion compounds. Masuda et al. reacted $BaTiO_{2.5}H_{0.5}$ with controlled amounts HF, to yield the mixed oxide-hydride-fluoride compound $BaTiO_{2.5}H_{0.25}F_{0.25}$ [40]. The closely related compound $BaTiO_{2.9}F_{0.1}$ has so far been reported only by the use of high temperature and pressure (3 GPa, 1300 °C) [50]. Further F^-/OH^- exchange is possible from here, as demonstrated by the preparation and characterization of $BaTiO_{2.4}D_{0.3}(OD)_{0.3}$ from $BaTiO_{2.4}D_{0.3}F_{0.3}$. This compound is an unusual case involving the co-existence of H^- and H^+ (or in actuality, D^- and D^+) within the same lattice, and has been made possible by the anion-exchange techniques starting from the labile oxyhydride precursor.

The two aforementioned reactions involve the direct exchange of H^- with other anions. However, even at higher temperatures where the hydride has already left, the remaining anion-deficient structure can be useful for further anion-exchange reactions. This has been demonstrated by the formation of $EuTiO_2N$ by Mikita et al. [41]. Here, $EuTiO_{2.82}H_{0.18}$ was first prepared. Treating with NH_3 at 400 °C resulted in direct N^{3-}/H^- exchange, to yield $EuTiO_{2.82}N_{0.1}\square_{0.06}$. Further treatment at 800 °C resulted in the further oxygen to be removed, despite no hydride being present, to yield $EuTiO_2N$. This contrasts with the reactivity of $EuTiO_3$, which shows no reactivity

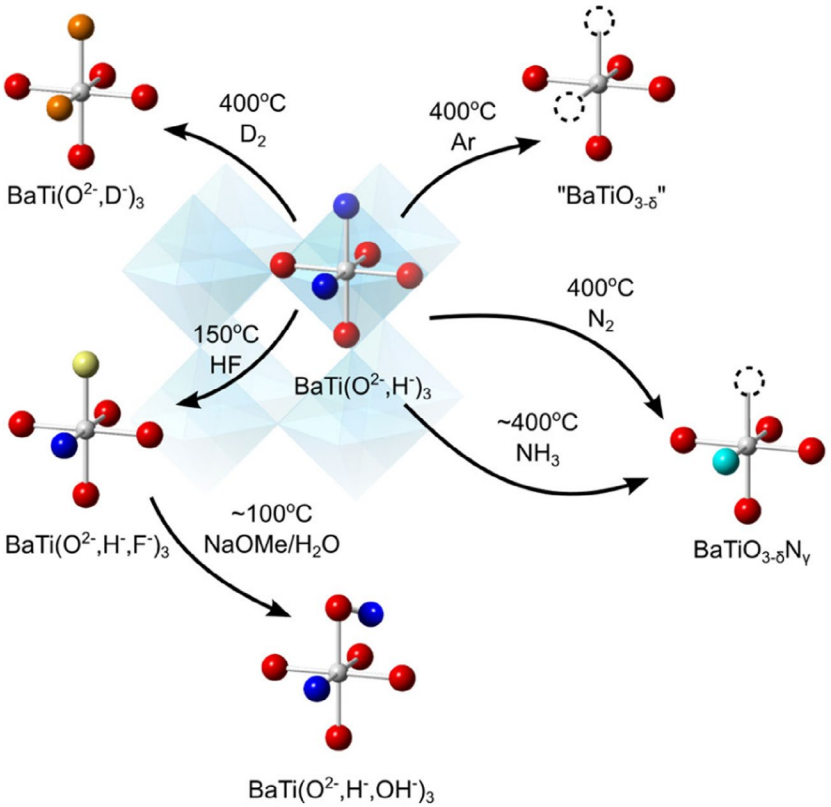

Figure 4. Different anion exchange routes starting from an oxyhydride.

with NH_3 even at 600 °C. Treatment of $EuTiO_3$ at 800 °C result in $EuTiO_{2.25}N_{0.75}$, but the composition $EuTiO_2N$ is not attained, unlike in the case when the oxyhydride was used as the starting material. This implies that the presence of the anionic vacancy during the reaction (2% in $EuTiO_{2.82}N_{0.1}\square_{0.06}$) has a significant impact on the anion-exchange reaction.

5. Physical properties in oxyhydrides: transport and magnetism

5.1. Titanate oxyhydride perovskites

The alkali earth titanate oxyhydrides exhibit semiconducting to metallic character, depending on the hydride doping amount. Loosely pressed pellets of powder $BaTiO_{3-x}H_x$ (100 nm) exhibit semiconducting temperature dependences with a room temperature conductivity of 4×10^{-4} S/cm. This is probably not the inherent behavior, though, as single crystal films deposited by pulsed laser deposition on substrates yielded comprehensive results, showing metallic behavior at high doping levels.

Yajima et al. and Bouilly et al. have examined the conductivity of various titanate perovskite oxyhydride films [31,32]. $SrTiO_{2.75}H_{0.25}$, $BaTiO_{2.36}H_{0.64}$, and $CaTiO_{2.32}H_{0.69}$ films on $(LaAlO_3)_{0.3}(SrAl_{0.5}Ta_{0.5}O_3)_{0.7}$ (LSAT) substrates showed high conductivities at room temperature, ranging from 10^2 to ~10^4 S/cm, and detailed temperature-dependent studies showed metallic behavior. The $SrTiO_{2.75}H_{0.25}$ films are somewhat analogous to previously reported $Sr(Ti_{0.8}Nb_{0.2})O_3$ films [51], in terms of doping level, carrier concentration, and conductivity, with both systems essentially being heavily *n*-doped systems. For the barium titanate system, one may compare the $BaTiO_{2.36}H_{0.34}$ films to reduced $BaTiO_3$. A key difference is that it is difficult to introduce a large number of oxygen vacancies in the perovskite structure due to structural instability, but extremely high doping levels can be achieved with hydride, as the anionic sites are always filled. The reduced $BaTiO_3$ films, with very small carrier concentrations, were metallic, with several ferroelectric transitions resulting in anomalies on ρ–T curves [52]. However, the $BaTiO_{2.36}H_{0.34}$ samples exhibited no such anomalies. The dependence of electrical properties on hydride content for $SrTiO_{3-x}H_x$ and $BaTiO_{3-x}H_x$ films has also been examined. While the Sr films always exhibit metallicity the Ba films are semiconducting at low hydride amounts. The reason for this may be the same as for Nb-doped $(Ba, Sr)TiO_{3-\delta}$, where incoherent displacement of Ti from the octahedral center led to increased electron scattering [53].

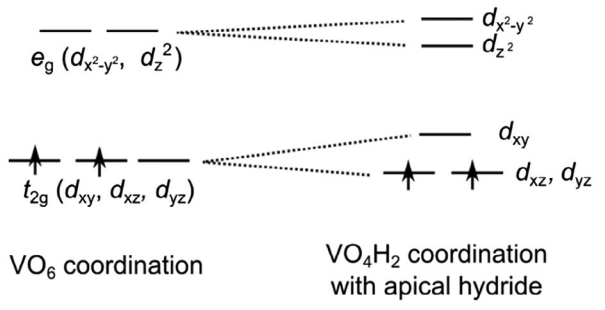

Figure 5. Molecular orbital diagram for $SrVO_2H$.

Another titanate oxyhydride, $EuTiO_{2.7}H_{0.3}$ has been synthesized [30]. Thin film studies also show metallic conductivity for this sample due to 3*d* electrons of Ti, induced from the hydride reduction. The *A*-site europium is in the +2 oxidation state, and has ferromagnetic order (T_c = 12 K) from spins on Eu 4*f* orbitals being mediated by itinerant Ti 3*d* electrons, in contrast to $EuTiO_3$ which is an antiferromagnetic insulator. The ferromagnetism based on the RKKY mechanism is also found in $Eu_{1-x}Ln_xTiO_3$ and $EuTi_{1-x}Cr_xO_3$, but here T_c is somewhat lower, implying the superiority of aliovalent hydride substitution at the anionic site in comparison with the cationic counterpart.

5.2. Vanadate oxyhydride perovskites and derivatives: $SrVO_2H$, Sr_2VO_3H, $Sr_3V_2O_5H_2$

The electronic and magnetic structures of $SrVO_2H$, and its related layered analogues, Sr_2VO_3H, and $Sr_3V_2O_5H_2$, (Figure 1(c), (f), and (g)) have been examined in detail [14,54,55]. These stoichiometric systems possess anion ordering, making them suitable for systematic studies. As shown in Figure 1(c), in the $SrVO_2H$ case, hydride occupies 'apical' sites (or *trans* octahedral VO_4H_2), whereas in the layered cases (Figure 1(f) and (g)), equatorial sites are occupied by hydride. Experimentally, neutron diffraction and muon spin relaxation shows that all three compounds have antiferromagnetic states. The Néel temperatures (T_N) are 170 and 240 K for Sr_2VO_3H and $Sr_3V_2O_5H_2$ [15]. Surprisingly, the Néel temperature of $SrVO_2H$ is well above room temperature despite the two-dimensional structure. Sr_2VO_3H and $Sr_3V_2O_5H_2$ are regarded, respectively, as quasi one- and two-dimensional magnets. The nearly temperature-independent susceptibility and the absence of anomalies near at the ordering temperatures may reflect the low-dimensional feature of these compounds, with short-ranged magnetic correlations being developed well above T_N [15].

The bonding and electronic structure in this system has been summarized by Romero et al. [15], Bang et al. [14] and Wei et al. [54], among others. A simple point is shown for $SrVO_2H$ in Figure 1(c). Here, H^- occupies the 'apical' site. For oxides such as $SrVO_3$, the t_{2g} orbitals would remain triply degenerate and each form π bonds with O 2*p* orbitals (Figure 5). Additionally, H^- cannot form π bonds since it consists of only *s* orbitals. Hence, given the hydride in the 'apical' position, the d_{xz} and d_{yz} orbitals experience less repulsion and decrease in energy, splitting the t_{2g} state into a doubly degenerate d_{xz} and d_{yz} bands with a d_{xy} band above. The two *d* electrons partially fill the lower d_{xz} and d_{yz} bands; calculations predict

the bands to have narrow dispersion, inducing a Mott transition to an insulator. This contrasts with the metallic $SrVO_3$, with band valence photoelectron spectroscopy on thin film samples confirming this difference [55]. The experimentally observed antiferromagnetic ordering has also been predicted by spin-polarized band structure calculations [54].

Recently, there has been much work concerning electronic doping VO_2 using various species. Doping VO_2 results in metal-insulator transitions, and so far oxide vacancies [56] and protons (H^+/e^-, via H_2 reduction) [57] have been introduced for *n*-doping to achieve alternate electronic states. Proton doping (via H_2 reduction) has the advantage of not inducing disorder, but hydride is unique given its *s* character, and should therefore be a valuable addition to the various tools available for the modulation of electronic states, which have recently been garnering attention [58,59].

5.3. Cobalt oxyhydride perovskite derivatives: $LaSrCoO_3H_{0.7}$, $Sr_3Co_2O_{4.33}H_{0.84}$

While the non-stoichiometric nature of the cobalt oxyhydrides has limited electronic structural calculations and thus close examination of electronic structure, the cobaltates, starting with $LaSrCoO_3H_{0.7}$, were the first reported transition metal oxyhydrides [8]. As shown in Figure 1(a), the structure of $LaSrCoO_3H_{0.7}$ is based a Ruddlesden–Popper layered perovskite, but with hydride anions and vacancies preferentially occupying select equatorial sites to form an orthorhombic lattice. As in the case of the previously mentioned vanadates, antiferromagnetic order is observed at room temperature, signifying that strong covalent interactions through the Co-H-Co chains, together with the larger magnetic moments, contribute to the enhanced T_N. $Sr_3Co_2O_{4.33}H_{0.84}$ (Figure 1(e)) is based on the n = 2 member of the Ruddlesden–Popper series [10]. While hydride has been incorporated, at this point oxygen removal is extensive, resulting in a mixture of tetrahedra and square pyramids. This extensive anion disorder and amount of vacancies is probably the reason for the lack of any observed magnetic order [10].

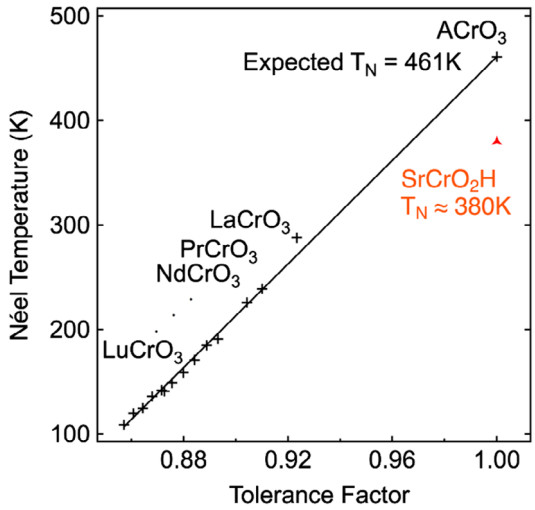

Figure 6. Change of Néel temperatures of various $RECrO_3$ (RE = rare earth) phases with the tolerance factor.

5.4. $SrCrO_2H$

The transition metal oxyhydride family was further expanded to chromates using high-pressure and high-temperature synthesis. $SrCrO_2H$ was prepared by heating powders of SrO, SrH_2 and Cr_2O_3 at 5 GPa and 1000 °C [16]. The successful synthesis of this material probably benefits from the high stability of the Cr^{3+} cation. Trivalent chromium oxides do not reduce even under harsh reducing conditions, allowing the high-pressure/high-temperature and hydride-rich environment sustainable for this species. The structure is cubic and its stoichiometry could be determined using a combination of X-ray and neutron diffraction, as previously used for $LaSrCoO_3H_{0.7}$. The oxide and hydride anions do not order in this structure, thus explaining the cubic structure. The magnetic properties of $SrCrO_2H$ were studied by variable-temperature NPD, revealing a G-type antiferromagnetic order with a Néel temperature as high as 380 K. The T_N observed in this system is much higher than those of isovalent $RECr^{III}O_3$ (RE = rare earth) structures with the highest previously known value for $LaCrO_3$ at T_N = 290 K. At a first glance, this behavior is strange as the octahedral environment in Cr^{3+} (t_{2g}^3) only allows π-type superexchange interactions (with the neighboring ligand) that cannot occur with the 1s orbital of the H^- anion. However, an hypothesis for this behavior is that the high symmetry of the $SrCrO_2H$ with a large Sr^{2+} cation (144 pm) gives a tolerance factor near 1; the cubic structure leads to ideal 180° Cr–O–Cr bond angles that allow strong superexchange antiferromagnetic interactions. In the case of oxide perovskites with smaller trivalent cations at the A site, distortions exist with tilting of the octahedra that leads to smaller T_N. As shown in Figure 6, the Néel temperature of Cr^{3+} perovskites increase linearly with the tolerance factor but $SrCrO_2H$ has a slightly lower than expected Néel temperature.

Liu and coworkers investigated the electronic and magnetic properties of $SrCrO_2H$ using DFT calculations on a hypothetical ordered trans-coordinated model isostructural with the reported $SrVO_2H$ [60]. In their study, the authors speculated a possible secondary effect where the hydride's lower electronegativity was partially responsible for the high T_N. The lower electronegativity of hydride should lead to delocalized orbitals along the Cr–H bonds, which in turn reinforces Cr–O bonds and strengthens the superexchange interactions along Cr–O–Cr paths.

5.5. $LaSrMnO_{3.3}H_{0.7}$

The synthesis of $LaSrMnO_3H_{0.7}$ was achieved via high pressure and high temperature at 5 GPa and 1000 °C on using powders of La_2O_3, MnO, Mn_2O_3, SrH_2 [17]. $LaSrMnO_{3.3}H_{0.7}$ crystallizes in the tetragonal *I*4/*mmm* space group with disorder of the oxide and hydride anions mainly in the equatorial plane (Figure 1(d)). This configuration confirms the trend observed also in cobaltate $LaSrCoO_3H_{0.7}$ and vanadates Sr_2VO_3H and $Sr_3V_2O_5H_2$. An important difference, however, lies in the lack of ordering of the two anions and therefore the observation of tetragonal symmetry rather than the orthorhombic symmetry found in the ordered Co and V systems. The anionic non-stoichiometry, determined by synchrotron X-ray and neutron diffraction, leads to a mixed valence Mn^{2+} and Mn^{3+} system with an average valence of $Mn^{2.3+}$. While magnetic susceptibility measurements confirm this valence, they also exhibit magnetic behavior suggesting a spin glass transition at T_{SG} = 22 K. The absence of magnetic Bragg reflections in the low temperature neutron diffraction is consistent with this spin glass picture. The negatively large value of a Curie–Weiss temperature θ = –149 K suggests the strong magnetic interactions. A fairly large frustration factor of $f \sim 6$ ($|\theta|/T_{SG}$) was discussed in terms of competing magnetic interactions between neighboring Mn cations, i.e. ferromagnetic Mn^{2+}–O–Mn^{3+} and antiferromagnetic Mn^{3+}–O–Mn^{3+} and Mn^{2+}–O–Mn^{2+}.

6. Crystallographic site selectivity of hydride in layered systems

Total or partial anion ordering has been the topic of many studies for a long time in various mixed anion transition metal materials isolated so far, including oxyhalides and oxynitrides. Besides DFT first-principles calculations, energy calculations (the Madelung part of the lattice energy) and the bond valence sum method, basics Pauling's electronegativity arguments have been evoked, whereby the more electronegative anion would be preferentially coordinated to the more electropositive cation, but without a total success in oxyfluorides, oxynitrides, or oxychlorides [61]. Another simple and general method for predicting the anion distribution not requiring the exact knowledge of the crystal structure has been proposed by Fuertes [62] according to the historic Pauling's Second Crystal Rule (PSCR) published in 1929 [63] as one of the principles governing the structure of complex ionic crystals. It is obviously assumed each cation is coordinated to anions at the corner of a polyhedron and vice versa. Those principles have been deduced from empirical knowledge of known crystal structure at that time, as well as from stability considerations in terms of crystal energy. Their application scope was limited by Pauling himself [63] as follows: small cations with relatively large electric charges (+3 or +4 typically) and crystal radii lower than about 0.8 Å; large univalent or divalent anions (over 1.35 Å) *not too highly deformable* such as oxygen or fluorine anions. Furthermore the chemical bonds in the crystal should not be of the 'extreme non-polar or shared electron pair type', thus excluding copper compounds and 'many other eighteen-shell atoms'. The PSCR or electrostatic valence principle [63] is based on the so-called strength *s* of the electrostatic valence bond (between one given cation and each adjacent anion) defined as $s = \frac{z}{\nu}$ where *z* is the formal charge of the cation and *ν* its coordination number (in anions). In a stable coordination structure, the formal charge –*ζ* of each anion (coordinated to *C* cations) approximately satisfies the following equation:

$$|\zeta| = \sum_{i=1}^{C} z_i/\nu_i = \sum_{i=1}^{C} s_i.$$

In materials (with anions of different charge) exhibiting chemically inequivalent anionic sites, for instance in lower than cubic symmetry layered perovskite structures, one can calculate according to the PSCR the charge –*ζ* of each anionic site that should be rather close to the charge of the anion actually occupying this site, allowing to predict the distribution of anions. Fuertes et al. [61,62] have shown this predictive method works well for many layered oxynitrides, oxyfluorides and oxychlorides (with the noteworthy exception of Nd_2AlO_3N [64], for which the difference between $\zeta_{equatorial}$ and ζ_{apical} calculated according to the PSCR, around 0.15, is very fine): the more charged anion would preferentially occupy the site showing the larger PSCR charge and conversely. Moreover for oxynitrides, oxyfluorides and one oxybromide of other structural types (e.g. antifluorite, baddeleyite, Th_3P_4, wurtzite …), PSCR appears as generally fulfilled though to a less extent for oxychlorides.

The discovery of $LaSrMnO_{3.3}H_{0.7}$ [17] by Tassel et al. has been naturally a motivation to confront this PSCR method with layered oxyhydride systems (including the previously published $LaSrCoO_3H_{0.7}$ [8], $NdSrCoO_{4-x}H_y$ [9], $PrSrCoO_{4-x}H_y$ [9] cobaltates or $Sr_2VO_{4-x}H_x$ vanadates [14,15] in order to check its applicability range over this new series of mixed anion systems. The PSCR calculated anion formal charge at the equatorial site appears as systematically higher than at the apical site (see Table 1), leading to a predicted apical site preference for H^- while in all the K_2NiF_4 transition metal oxyhydrides hydride

Table 1. Formal charge of the apical and equatorial anionic site in known K_2NiF_4 transition metal oxyhydrides calculated according to the Pauling's Second Crystal Rule (PSCR).

Oxyhydride	ζ_{apical}	$\zeta_{equatorial}$
$LaSrMnO_{3.3}H_{0.7}$	–1.61	–1.89
$LaSrCoO_3H_{0.7}$	–1.67	–1.68
$NdSrCoO_{4-x}H_y$	–1.67	–1.68
$PrSrCoO_{4-x}H_y$	–1.67	–1.68
$Sr_2VO_{4-x}H_x$	–1.77	–1.88

Table 2. Summary of transition metal oxyhydride compounds.

Compound	Preparation*	Properties*	Anion arrangement*	Reference
$LaSrCoO_3H_{0.7}$	CaH_2	I; AFM (T_N > RT); H^- diffusion	Partial order, eq.	[8,33,45]
$NdSrCoO_{3.1}H_{0.80}$, $NdSrCoO_{3.21}H_{0.58}$	CaH_2	AFM (T_N = 410 K) AFM (T_N = 375 K)	Partial order, eq.	[9]
$PrSrCoO_{3.16}H_{0.68}$	CaH_2	AFM (T_N = 445 K)	Partial order, eq.	[9]
$Sr_3Co_2O_{4.33}H_{0.84}$	CaH_2	PM	Partial order, eq.	[10]
$(Ca, Ba, Sr)TiO_{3-x}H_x$	CaH_2	MS; PM	Random	[29,31,32]
$EuTiO_{3-x}H_x$	CaH_2	M; FM from Eu moments (T_c = 12 K)	Random	[30]
$Ln_2Ti_2O_{7-x}H_x$	CaH_2	Electrocatalysis	Unknown (trace)	[37]
$SrVO_2H$	CaH_2	I; AFM (T_N > RT)	Ordered, apical	[15,55]
Sr_2VO_3H	CaH_2	I; AFM (T_N = 170 K)	Ordered, equatorial	[15]
$Sr_2VO_{3-x}H_x$	HP		Partial order, eq.	[14]
$Sr_3V_2O_5H_2$	CaH_2	I; AFM (T_N = 240 K)	Ordered, equatorial	[15]
$SrCrO_2H$	HP	I; AFM (T_N = 380 K)	Random	[16]
$LaSrMnO_{3.3}H_{0.7}$	HP	I; SG (T_{SG} = 22 K)	Partially ordered	[17]
$BaScO_2H$	HP	I; local order (^{1}H NMR, DFT)	Random	[13]

*CaH_2 = reduction with CaH_2, HP = high pressure, AFM = antiferromagnetism, FM = ferromagnetism, PM = paramagnetism, SG = spin glass, eq. = equatorial, I = insulating, M = metallic, S = semiconducting.

anions are located only on the equatorial site, except to be complete the case of $Sr_2VO_{3.62}H_{0.38}$ and $Sr_2VO_{2.99}H_{1.01}$ [14] though extremely low chemical occupancy of respectively 4 and 1.5% for H^- are suggested on the apical site (vs. 15 and 93%/5% on the equatorial site(s)). Hence it turns out the PSCR is not able to predict the anion ordering in transition metal oxyhydrides. However it should be stressed that the difference between PSCR $\zeta_{equatorial}$ and ζ_{apical} remains small for all the highlighted examples of Table 1, reaching at best 0.28.

One singularity of hydride anion that could also explain the violation of the PSCR in oxyhydrides is its small Pauling's electronegativity (2.1), as low as astatine, 2.2, the rare heaviest halogen, that may be too small for an electrostatic-based principle. It is worth noticing the lowest electronegative anion used by Fuertes et al. [61,62] to support the PSCR is bromine (χ = 2.96). Also hydride is highly polarizable and shows in crystals an ill-defined size ranging from 1.35 to 1.53 Å depending on the covalent to ionic bond character with a metal [65], property that strongly contradicts PSCR's prerequisites underlined above in terms of non-deformability of anions.

Ordering/disordering of hydride within the equatorial plane of layered oxyhydrides has been controlled by Bouilly et al. [33] in epitaxial thin films through the use of different orientations of the LSAO ($LaSrAlO_4$) substrate leading to two orientations (perpendicular or parallel) of the layer *c*-axis of the oxyhydride with respect to the substrate. CaH_2-topochemical conversion of the *c*-axis and *b*-axis oriented $LaSrCoO_4$ films (deposited by pulsed laser deposition on LSAO (0 0 1) and LSAO (1 0 0) substrates, respectively) leads to $LaSrCoO_3H_{0.7}$ oxyhydride films with tetragonal and orthorhombic symmetry, respectively. The latter and former cases correspond respectively to a crystallographically ordered and disordered hydride/oxide arrangement within the equatorial plane (see Figure 1(a) of [33]). In other words, the anionic order observed in bulk $LaSrCoO_3H_{0.7}$ [34] is recovered when the precursor oxide is deposited on the LSAO with *c*-axis within the film surface, while remarkably an original hydride/oxide disorder is created within the equatorial plane when the precursor oxide is deposited with a *c*-axis perpendicular to the film surface. These results demonstrate that strain engineering can lead to new materials with designed anion arrangement in mixed anion materials.

7. Summary and outlook

As discussed in this review, oxyhydrides have gone through rapid development over the past 10 years. We have summarized the various compounds and their characteristics in Table 2. Among the 3*d* transition metals, only Fe, Cu, and Zn oxyhydrides remain to be discovered. In terms of properties, hydride has certain characteristics unlike any other mixed anions. The 1*s* character gives it unusual bonding and hence magnetic/electronic implications, and may be useful in controlling the electronic properties of various materials with applications in devices. In terms of ionic conductivity, recently, reports on pure hydride ion conductivity for layered non-transition metal hydride perovskites have been reported [66], opening the doorway to hydride-based ionics. One can even imagine high-potential electrochemical cells based on the H^-/H^+ redox couple; such applications would not be possible without a wide range of hydride-based materials to choose from. We have also discussed the chemical lability of hydride, and this may serve as a useful approach to new hydrogenation catalysts based on (oxy-) hydrides. With these potential applications in devices, ionics, and catalysis, together with their fundamental scientific impact, it is evident that transition metal oxyhydrides will continue to gain prominence in the future.

Acknowledgements

A significant portion of this work was assisted by the Japan–France Bilateral Joint Research Project from the Japan Society for the Promotion of Science (JSPS), and the Centre

National de la Recherche Scientifique, (CNRS), [PRC No. 0684 2013-2014].

Disclosure statement

No potential conflict of interest was reported by the authors.

Funding

This work was supported by the CREST [No. JPMJCR1421] program from the Japan Science and Technology Agency (JST); and Grant-in-Aid for Scientific Research on Innovative Areas 'Mixed anion' [JP16H06439] from MEXT.

References

[1] Norby T, Widerøe M, Glöckner R, et al. Hydrogen in oxides. Dalton Trans. 25;2004:3012–3018

[2] Brice JF, Moreau A. Synthèse et conductivité anionique des hydruro-oxydes de lanthane de formule LaHO, $LaH_{1+2x}O_{1-x}$ et $LaH_{1+y}O_{1-x}$ (y < 2x). Ann Chim Fr. 1982;7:623–634.

[3] Malaman B, Brice JF. Étude structurale de l'hydruro-oxyde LaHO par diffraction des rayons X et par diffraction des neutrons. J Solid State Chem. 1984;53:44–54.

[4] Rotella FJ, Flotow HE, Gruen DM, et al. Deuterium site occupation in the oxygen-stabilized η-carbides $Zr_3V_3OD_x$. I. Preparation and neutron powder diffraction. J Chem Phys. 1983;79:4522–4531.

[5] Clark NJ, Wu E. Hydrogen absorption by M_5X_3 phase Zr-Al compounds. J Less Common Metals. 1988;142:145–154.

[6] Huang B, Corbett JD. Ba_3AlO_4H: synthesis and structure of a new hydrogen-stabilized phase. J Solid State Chem. 1998;141:570–575.

[7] Huang B, Corbett JD. $Ba_{21}Ge_2O_5H_{24}$ and related phases. A corrected structure type and composition for a Zintl phase stabilized by hydrogen. Inorg Chem. 1998;37:1892–1899.

[8] Hayward MA, Cussen EJ, Claridge JB, et al. The hydride anion in an extended transition metal oxide array: $LaSrCoO_3H_{0.7}$. Science. 2002;295:1882–1884.

[9] Bowman A, Claridge JB, Rosseinsky MJ. Anion composition control and magnetic short- and long-range order in transition metal oxide hydrides. Chem Mater. 2006;18:3046–3056.

[10] Helps RM, Rees NH, Hayward MA. $Sr_3Co_2O_{4.33}H_{0.84}$: an extended transition metal oxide-hydride. Inorg Chem. 2010;49:11062–11068.

[11] Poulsen FW. Speculations on the existence of hydride ions in proton conducting oxides. Solid State Ionics. 2001;145:387–397.

[12] Kobayashi Y, Hernandez OJ, Sakaguchi T, et al. An oxyhydride of $BaTiO_3$ exhibiting hydride exchange and electronic conductivity. Nat Mater. 2012;11:507–511.

[13] Goto Y, Tassel C, Noda Y, et al. Pressure-stabilized cubic perovskite oxyhydride $BaScO_2H$. Inorg Chem. 2017;56:4840–4846.

[14] Bang J, Matsuishi S, Hiraka H, et al. Hydrogen ordering and new polymorph of layered perovskite oxyhydrides: $Sr_2VO_{4-x}H_x$. J Am Chem Soc. 2014;136:7221–7224.

[15] Romero DF, Leach A, Möller JS, et al. Strontium vanadium oxide-hydrides: "square-planar" two-electron phases. Angew Chem Int Ed Engl. 2014;53:7556–7559.

[16] Tassel C, Goto Y, Kuno Y, et al. Direct synthesis of chromium perovskite oxyhydride with a high magnetic-transition temperature. Angew Chem Int Ed. 2014;53:10377–10380.

[17] Tassel C, Goto Y, Watabe D, et al. High-pressure synthesis of manganese oxyhydride with partial anion order. Angew Chem Int Ed Engl. 2016;128:9819–9822.

[18] Hayward MA, Green MA, Rosseinsky MJ, et al. Sodium hydride as a powerful reducing agent for topotactic oxide deintercalation: synthesis and characterization of the nickel(I) oxide $LaNiO_2$. J Am Chem Soc. 1999;121:8843–8854.

[19] Seddon J, Suard E, Hayward MA. Topotactic reduction of $YBaCo_2O_5$ and $LaBaCo_2O_5$: square-planar Co(I) in an extended oxide. J Am Chem Soc. 2010;132:2802–2810.

[20] Dixon E, Hadermann J, Ramos S, et al. Mn(I) in an extended oxide: the synthesis and characterization of $La_{1-x}Ca_xMnO_{2+\delta}$ ($0.6 \leq x \leq 1$). J Am Chem Soc. 2011;133:18397–18405.

[21] Romero FD, Coyle L, Hayward MA. Structure and magnetism of $Sr_3Co_2O_4Cl_2$ an electronically driven lattice distortion in an oxychloride containing square planar Co^{II} centers. J Am Chem Soc. 2012;134:15946–15952.

[22] Tsujimoto Y, Tassel C, Hayashi N, et al. Infinite-layer iron oxide with a square-planar coordination. Nature. 2007;450:1062–1065.

[23] Tassel C, Pruneda JM, Hayashi N, et al. $CaFeO_2$: a new type of layered structure with iron in a distorted square planar coordination. J Am Chem Soc. 2009;131:221–229.

[24] Tassel C, Watanabe T, Tsujimoto Y, et al. Stability of the infinite layer structure with iron square planar coordination. J Am Chem Soc. 2008;130:3764–3765.

[25] Yamamoto T, Li Z, Tassel C, et al. Synthesis and thermal stability of the solid solution $AFeO_2$ (A = Ba, Sr, Ca). Inorg Chem. 2010;49:5957–5962.

[26] Seinberg L, Yamamoto T, Tassel C, et al. Fe-site substitution effect on the structural and magnetic properties in $SrFeO_2$. Inorg Chem. 2011;50:3988–3995.

[27] Poltavets VV, Lokshin KA, Dikmen S, et al. $La_3Ni_2O_6$: a new double T'-type nickelate with infinite $Ni^{1+/2+}O_2$ layers. J Am Chem Soc. 2006;128:9050–9051.

[28] Hadermann J, Abakumov AM, Adkin JJ, et al. Topotactic reduction as a route to new close-packed anion deficient perovskites: structure and magnetism of 4H-$BaMnO_{2+x}$. J Am Chem Soc. 2009;131:10598–10604.

[29] Sakaguchi T, Kobayashi Y, Yajima T, et al. Oxyhydrides of (Ca, Sr, Ba)TiO_3 perovskite solid solutions. Inorg Chem. 2012;51:11371–11376.

[30] Yamamoto T, Yoshii R, Bouilly G, et al. An antiferro-to-ferromagnetic transition in $EuTiO_{3-x}H_x$ induced by hydride substitution. Inorg Chem. 2015;54:1501–1507.

[31] Yajima T, Kitada A, Kobayashi Y, et al. Epitaxial thin films of $ATiO_{3-x}H_x$ (A = Ba, Sr, Ca) with metallic conductivity. J Am Chem Soc. 2012;134:8782–8785.

[32] Bouilly G, Yajima T, Terashima T, et al. Electrical properties of epitaxial thin films of oxyhydrides $ATiO_{3-x}H_x$ (A= Ba and Sr). Chem Mater. 2015;27:6354–6359.

[33] Bouilly G, Yajima T, Terashima T, et al. Substrate-induced anion rearrangement in epitaxial thin films of $LaSrCoO_{4-x}H_x$. CrystEngComm. 2014;16:9669–9674.

[34] Hayashi K, Matsuishi S, Kamiya T, et al. Light-induced conversion of an insulating refractory oxide into a

persistent electronic conductor. Nature. 2002;419:462–465.
[35] Hayashi K. Heavy doping of H^- ion in 12CaO $7Al_2O_3$. J Solid State Chem. 2011;184:1428–1432.
[36] Kitada A, Kasahara S, Terashima T, et al. Highly reduced anatase $TiO_{2-\delta}$ thin films obtained via low-temperature reduction. Appl Phys. Express. 2011;4:035801.
[37] Pussacq T, Kabbour H, Colis S, et al. Reduction of $Ln_2Ti_2O_7$ layered perovskites: a survey of the anionic lattice, electronic features, and potentials. Chem Mater. 2017;29:1047–1057.
[38] Kobayashi Y, Li Z, Hirai K, et al. Gas phase contributions to topochemical hydride reduction reactions. J Solid State Chem. 2013;207:190–193.
[39] Hayashi K, Sushko PV, Hashimoto Y, et al. Hydride ions in oxide hosts hidden by hydroxide ions. Nat Commun. 2014;5:1–8.
[40] Masuda N, Kobayashi Y, Hernandez O. Hydride in $BaTiO_{2.5}H_{0.5}$: a labile ligand in solid state chemistry. J Am Chem Soc. 2015;137:15315–15321.
[41] Mikita R, Aharen T, Yamamoto T, et al. Topochemical nitridation with anion vacancy-assisted N^{3-}-/O^{2-}-exchange. J Am Chem Soc. 2016;138:3211–3217.
[42] Izumi F, Momma K. 2011 Three-dimensional visualization of electron-and nuclear-density distributions in inorganic materials by MEM-based technology. In: IOP Conference Series: Materials Science and Engineering. Vol. 18. IOP Publishing. p. 022001
[43] Yoshizumi T, Kobayashi Y, Kageyama H, et al. Simultaneous quantification of hydride ions and electrons incorporated in 12CaO $7Al_2O_3$ cages by deuterium-labeled volumetric analysis. J Phys Chem C. 2012;116:8747–8752.
[44] Castro FJ, Meyer G. Thermal desorption spectroscopy (TDS) method for hydrogen desorption characterization (I): theoretical aspects. J Alloys Compd. 2002;330–332:59–63.
[45] Bridges CA, Fernandez-Alonso F, Goff JP, et al. Observation of hydride mobility in the transition-metal oxide hydride $LaSrCoO_3H_{0.7}$. Adv Mater. 2006;18:3304–3308.
[46] Lu X, Cheung NW, Strathman MD, et al. Hydrogen induced silicon surface layer cleavage. Appl Phys Lett. 1997;71:1804–1806.
[47] Sandim HRZ, Morante BV, Suzuki PA. Kinetics of thermal decomposition of titanium hydride powder using *in situ* high-temperature X-ray diffraction (HTXRD). Mater Res. 2005;8:293–297.
[48] Liu H, He P, Feng JC, et al. Kinetic study on nonisothermal dehydrogenation of TiH_2 powders. Int J Hydrogen Energy. 2009;34:3018–3025.
[49] Yajima T, Takeiri F, Aidzu K, et al. A labile hydride strategy for the synthesis of heavily nitridized $BaTiO_3$. Nat Chem. 2015;7:1017–1023.
[50] Endo T, Kobayashi T, Sato T, et al. High pressure synthesis and electrical properties of $BaTiO_{3-x}F_x$. J Mater Sci. 1990;25:619–623.
[51] Ohta H, Sugiura K, Koumoto K. Recent progress in oxide thermoelectric materials: p-type $Ca_3Co_4O_9$ and n-type $SrTiO_3$. Inorg Chem. 2008;47:8429–8436.
[52] Kolodiazhnyi T. Insulator-metal transition and anomalous sign reversal of the dominant charge carriers in perovskite $BaTiO_{3-\delta}$. Phys Rev B: Condens Matter Mater Phys. 2008;78:045107.
[53] Page K, Kolodiazhnyi T, Proffen T, et al. Local structural origins of the distinct electronic properties of Nb-substituted $SrTiO_3$ and $BaTiO_3$. Phys Rev Lett. 2008;101:205502.
[54] Wei Y, Gui H, Li X, et al. The effect of hydrogen ordering on the electronic and magnetic properties of the strontium vanadium oxyhydride. J Phys Condens Matter. 2015;27:206001.
[55] Katayama T, Chikamatsu A, Yamada K, et al. Epitaxial growth and electronic structure of oxyhydride $SrVO_2H$ thin films. J Appl Phys. 2016;120:085305.
[56] Zhang Z, Zuo F, Wan C, et al. Evolution of metallicity in vanadium dioxide by creation of oxygen vacancies. Phys Rev Appl. 2017;7:034008.
[57] Yoon H, Choi M, Lim T-W, et al. Reversible phase modulation and hydrogen storage in multivalent VO_2 epitaxial thin films. Nat Mater. 2016;15:1113–1119.
[58] Shi J, Zhou Y, Ramanathan S. Colossal resistance switching and band gap modulation in a perovskite nickelate by electron doping. Nat Commun. 2014;5:1–9.
[59] Lu N, Zhang P, Zhang Q, et al. Electric-field control of tri-state phase transformation with a selective dual-ion switch. Nature. 2017;546:124–128.
[60] Liu K, Hou Y, Gong X, et al. Orbital delocalization and enhancement of magnetic interactions in perovskite oxyhydrides. Sci Rep. 2016;6:1–7.
[61] Tobías G, Beltrán-Porter D, Lebedev OI, et al. Anion ordering and defect structure in Ruddlesden-Popper strontium niobium oxynitrides. Inorg Chem. 2004;43:8010–8017.
[62] Fuertes A. Prediction of anion distributions using Pauling's second rule. Inorg Chem. 2006;45:9640–9642.
[63] Pauling L. The principles determining the structure of complex ionic crystals. J Am Chem Soc. 1929;51:1010–1026.
[64] Marchand R, Pastuszak R, Laurent Y. Structure cristalline de Nd_2AlO_3N. Détermination de L'ordre oxygène-azote par diffraction de neutrons. Rev Chim. 1982;19:684–689.
[65] Morris DFC, Reed GL, Pauling L. Crystal radius of the hydride ion. J Inorg Nucl Chem. 1965;27:1715–1717.
[66] Kobayashi G, Hinuma Y, Matsuoka S, et al. Pure H^- conduction in oxyhydrides. Science. 2016;351:1314–1317.